Adv Polym Sci (2006) 200: 91–117
DOI 10.1007/12_038
© Springer-Verlag Berlin Heidelberg 2005
Published online: 6 December 2005

# Surface Nano- and Microstructuring with Organometallic Polymers

Igor Korczagin · Rob G. H. Lammertink · Mark A. Hempenius · Steffi Golze · G. Julius Vancso (✉)

University of Twente, MESA+ Institute for Nanotechnology, P.O. Box 217,
7500 AE Enschede, The Netherlands
*g.j.vancso@tnw.utwente.nl*

1 **Introduction** . . . . . . 92

2 **Poly(ferrocenyldimethylsilane) as a Reactive Ion Etch Barrier** . . . . . . 94

3 **Lithographic Applications of Poly(ferrocenylsilane) Homopolymers** . . . . 97
3.1 Printing of Organometallic Polymers by Soft Lithography . . . . . . 97
3.2 Directed Dewetting . . . . . . 99
3.3 Capillary Force Lithography . . . . . . 100

4 **Lithographic Applications of Poly(ferrocenylsilane) Block Copolymers** . . 102
4.1 Structure Formation via Block Copolymer Self-Assembly . . . . . . 102
4.2 Block Copolymer Thin Films . . . . . . 104
4.3 Self-Assembling Resists . . . . . . 106

5 **Guided Deposition of Poly(ferrocenylsilane) Polyions** . . . . . . 108

6 **Conclusions** . . . . . . 113

**References** . . . . . . 114

**Abstract** This paper gives an overview of the use of poly(ferrocenylsilane)s in the surface patterning of silicon substrates. Due to the presence of iron and silicon in their main chain, poly(ferrocenylsilane)s show a very high resistance to reactive ion etching, allowing one to transfer polymer patterns directly onto the substrate. Methods for introducing etch-resistant polymer patterns on substrate surfaces include soft lithography approaches such as microcontact printing, directed dewetting, and capillary force lithography. Next to top-down methods, self-assembly strategies are discussed. Phase separation in thin films of asymmetric organic–organometallic block copolymers leads to the formation of nanoperiodic organometallic patterns. The use of such thin films as nanolithographic templates is demonstrated. Surface patterning can also be realized using electrostatic self-assembly of organometallic polyions. Layer-by-layer deposition of poly(ferrocenylsilane) polyanions and polycations on chemically patterned substrates allows one to guide the growth of multilayer thin films and to produce patterned organometallic coatings.

**Keywords** Block copolymers · Etch resistance · Nanolithography · Organometallic polymers · Thin films

# 1 Introduction

Macromolecules featuring inorganic elements or organometallic units in the main chain are of considerable interest as they may combine potentially useful chemical, electrochemical, optical, and other interesting characteristics with the processability of polymers [1, 2]. Poly(ferrocenylsilane)s (PFSs), composed of alternating ferrocene and silane units in the main chain, belong to the class of organometallic polymers. The presence of iron and silicon in the PFS backbone adds a distinctive functionality to this class of materials [3]. Poly(ferrocenylsilane)s were found to be effective resists in reactive ion etching processes due to the formation of an etch-resistant iron/silicon oxide layer in oxygen plasmas [4], resulting in several lithographic applications of PFSs. Patterns on micron and sub-micron scales were obtained using PFSs as ink in various soft lithographic techniques [5], and nanopatterning was realized by means of block copolymer lithography. Block copolymers featuring poly(ferrocenylsilane) blocks form nanoperiodic microdomain structures upon phase separation [6]. In thin films of such block copolymers, e.g., poly(isoprene-*block*-ferrocenyldimethylsilane), the high resistance of the organometallic phase to reactive ion etching compared to the organic phase was used to form nanopatterned surfaces. These patterns were transferred onto silicon or silicon nitride substrates in a one-step etching process [7]. Ferrocenylsilane block copolymers can even be employed to pattern thin metal films, as was demonstrated by the use of ferrocenylsilane-styrene block copolymers as templates in the fabrication of nanometer-sized cobalt magnetic dot arrays [8]. Furthermore, phase-separated block copolymer thin films containing PFS domains were found to be efficient precursors to nanoperiodic arrays of iron oxide particles that are active catalysts in the growth of carbon nanotubes [9, 10]. The presence of ferrocene units in the main chain renders PFS electrochemically active [11]. Reversible redox-induced morphology and volume/thickness changes were observed in self-assembled poly(ferrocenylsilane) monolayers on gold [12, 13]. These effects are intimately related to the changes in solubility and conformation of the PFS macromolecules upon oxidation and reduction. Thus, surface-immobilized PFSs constitute an interesting electrochemically addressable stimulus-responsive system [14]. The redox activity of PFS was also employed in the preparation of a redox- and solvent-tunable photonic crystal. The material used in this device was composed of silica microspheres in a matrix of crosslinked PFSs. The geometry and optical properties of the crystal could be changed using the chemomechanical response of PFSs [15].

Pyrolysis of PFS polymers yields nanocomposites containing magnetic Fe clusters with tunable magnetic properties [16]. Finally, block copolymers containing PFS blocks self-assemble, generating remarkable nanoarchitectures such as cylindrical micelles in selective solvents [17, 18]. Con-

sequently, these block copolymers are interesting candidates for a range of potential applications from the fabrication of nanostructured magnetic materials to electronic and photonic applications.

Poly(ferrocenylsilane)s were first obtained by Rosenberg in a condensation polymerization of an appropriate biscyclopentadienide anion with iron(II)chloride [19]. This resulted in oligomers with degrees of polymerization of up to 10. An important step in the development of these polymers was the discovery by Manners et al. that strained, silicon-bridged[1]ferrocenophanes undergo thermal ring-opening polymerization, producing high-molar-mass PFSs [20]. Furthermore, sila[1]ferrocenophanes were found to be polymerizable in solution, by using anionic initiators [21] or transition metal catalysts [22, 23], or in the solid state using a $^{60}$C $\gamma$-ray source [24] (Scheme 1).

The macromolecular characteristics of the resulting polymers depend on the substituents at silicon. Polymerization of asymmetrically substituted sila[1]ferrocenophanes [25] yields amorphous polymers while symmetrically substituted ferrocenophanes yield semicrystalline materials [26]. Additionally, the glass transition temperature of PFSs can be tuned by varying the size and type of the substituents [27–29]. Several types of iron-containing macromolecules have been synthesized by polymerizing ferrocenophanes with varying numbers and types of bridging atoms [30] and substituents on the cyclopentadienyl rings [31]. The synthesis of water-soluble PFS polyanions [32–34] and polycations [35, 36] and their layer-by-layer deposition [36, 37] to form multilayer thin films was also reported.

The discovery of the anionic ring-opening polymerization of silicon-bridged[1]ferrocenophanes enabled the synthesis of well-defined, near-monodisperse poly(ferrocenylsilane) homo- and block copolymers. PFS was combined with polystyrene [38], polyisoprene [39], poly(dimethylsiloxane) [40], poly(ethylene oxide) [41], poly(ferrocenylphenylphosphine) [42], poly(aminoalkyl methacryate) [43] and recently with poly(methyl methacrylate) [44, 45] blocks.

In the following sections, methods for introducing poly(ferrocenylsilane) patterns on silicon substrates are discussed. These methods include soft lithography approaches such as microcontact printing and capillary force lithography and the self-organization of organic–organometallic block copolymers in thin films, allowing one to form nanoperiodic organometallic patterns, which

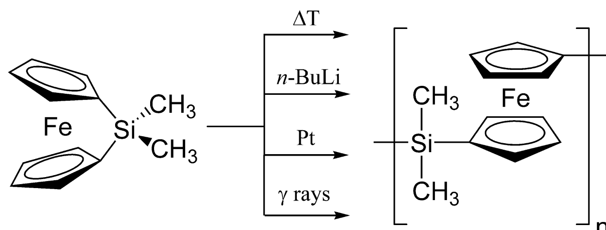


**Scheme 1** Ring-opening polymerization of strained dimethylsila[1]ferrocenophane

can serve as nanolithographic templates. Finally, the electrostatic self-assembly of poly(ferrocenylsilane) polyanions and polycations will be discussed as a means to area-selectively introduce ultrathin poly(ferrocenylsilane) films on chemically patterned substrates.

## 2 Poly(ferrocenyldimethylsilane) as a Reactive Ion Etch Barrier

Oxygen and oxygen-containing plasmas are most commonly employed to modify polymer surfaces [46]. Reactive ion etching can be divided into two etching processes; namely, chemical and physical [47]. Chemical etching refers to the chemical reactions that take place between the active plasma species and the surface of interest. After absorption of the reactive species, the reaction takes place, and the product desorbs from the surface. Physical etching occurs due to the bombardment of positive ions. The positive ions are accelerated towards the surface and break bonds upon impact, which results in physical etching. The balance between the two etching mechanisms depends on many variables, such as gas pressure and composition, reactor design, and temperature [48, 49].

Organometallic compounds are known to act as etching barriers in oxygen plasmas. Contrary to organic compounds, products of chemical etching with oxygen plasmas are non-volatile and therefore do not desorb from the surface. This is the fundamental reason for the low etch rates found for inorganic species when using oxygen plasmas. When poly(ferrocenylsilane) films are exposed to oxygen reactive ion etching conditions, a thin Fe/Si-oxide layer is formed on top of the film, as was established by XPS [4].

From Auger electron spectroscopy (AES), using argon ion-sputtering depth profiling, the composition in the depth of the PFS film was investigated. In the AES spectra (Fig. 1), the first sputtering cycle corresponds to the sample surface, and the increase of the Si signal around cycle 90 indicates the underlying substrate. A thin oxide-rich layer of approximately 10 nm is present at the surface. Compared to the film interior, relatively little carbon and a significant amount of oxygen are present at the surface oxide layer. Interestingly, more silicon is removed from the surface compared to iron in the oxygen plasma treatment.

Radio-frequency discharges in low-pressure fluorocarbon gases are often used for etching silicon, silicon oxide, and silicon nitride [50, 51]. Gases commonly employed in reactive ion etching are $CF_4$, $CHF_3$, $C_2F_6$, $SF_6$, etc. [52]. By adjusting the composition of the gas, the nature of the plasma can be dramatically changed [53]. Although the process of etching with such plasmas is very complex, and diverse variants of the process exist, some general observations can be highlighted. The C/F atomic ratio of the feed gas is a crucial parameter for the nature of the plasma [54]. If the C/F atomic ratio of the

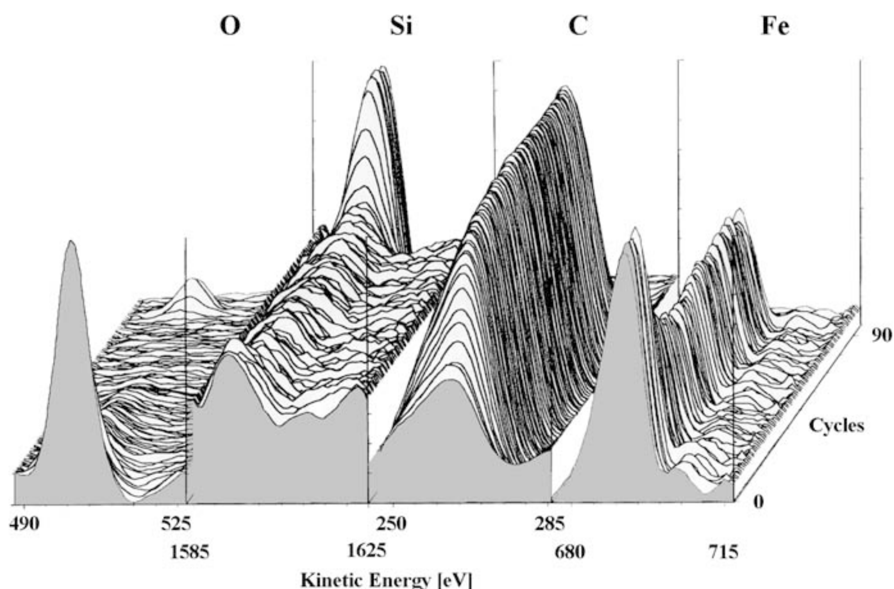


**Fig. 1** Auger electron spectroscopy depth profile of an oxygen-plasma-treated film of poly(ferrocenyldimethylsilane). The front of the image corresponds to the exposed free surface. Reproduced with permission from [4]. Copyright 2001, American Chemical Society

feed-in gas increases, the concentration of CF and $CF_2$ radicals will be higher at the expense of F, and the plasma becomes "polymerizing" and hence protective rather than "etching" due to deposition of a thin fluorocarbon polymer film on the substrate [55, 56]. Even a very thin fluorocarbon film deposited on the substrate results in significant reduction of the $SiO_2$ etch rate. To suppress this so-called etch stop, the fluorocarbon gases have been diluted with other gases like oxygen [57–59]. Oxygen atoms act as scavengers for carbon, and consequently a relative higher [F] (the etching component) rather than $[CF_x]$ (the polymerizing component) is obtained. Figure 2 shows an example of a structured silicon wafer produced by exposure to $CF_4/O_2$ reactive ion etching (RIE), using a PFS mask prepared by capillary force lithography [5]. Under the employed conditions, the etch rate contrast between PFS resist and silicon substrate is on the order of 10 : 1.

In order to fabricate structures with higher aspect ratios, one has to decrease sputtering action, which might affect the polymeric mask and increase the rate of chemical etching of the substrate. This has to be achieved without compromising the anisotropy of the etching process. By using $SF_6$ as the etch gas in a cryogenic reactive ion etcher, where the physical and chemical etching parameters could be varied independently, we could optimize conditions for the highest etch rate contrast [60]. The substrate temperature was kept at – 110 °C during processing. As a result, the rate of chemical etching for Si in-

creased and the rate of physical sputtering was drastically reduced. Using this process we obtained etch rates of 3000 nm/min into Si and around 5 nm/min in the PFS layer (etch rate contrast of 600 : 1). A typical cross-section of an etched stripe pattern is shown in Fig. 3. Such a high etch rate contrast enables the fabrication of high-aspect-ratio structures. Silicon nanopillars with aspect ratios of 10 (see Fig. 4) were obtained with ease.

As the potential of poly(ferrocenyldimethylsilane) as an etch barrier has been demonstrated, we now focus on pathways to generate patterns of these

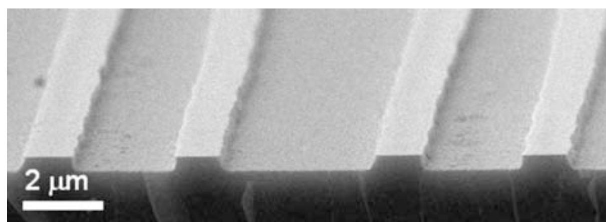


**Fig. 2** SEM image of a patterned silicon substrate. Lines of poly(ferrocenylmethylphenylsilane) were introduced by capillary force lithography, followed by $CF_4/O_2$ reactive ion etching (10 min). The polymer mask was subsequently removed using nitric acid

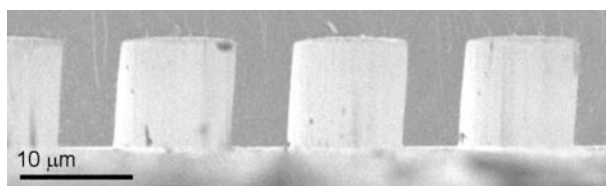


**Fig. 3** Cross-sectional SEM image of a patterned silicon substrate. By means of micromolding in capillaries (MIMIC), Si was decorated with poly(ferrocenyldimethylsilane) lines, followed by etching with $SF_6$ (3 min) in a cryogenic reactive ion etcher. The organometallic polymer residue was removed with nitric acid

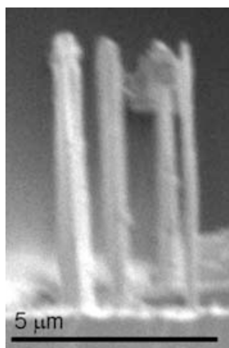


**Fig. 4** SEM image of silicon nanopillars obtained using cryogenic RIE and a poly(ferrocenyldimethylsilane) mask. The substrate was etched with $SF_6$ (2 min)

polymers. Masking layers with a high etch resistance are potentially useful for very thin resist layer applications, since reducing resist film thickness is a viable method to prevent pattern collapse when fabricating high-aspect-ratio structures.

## 3 Lithographic Applications of Poly(ferrocenylsilane) Homopolymers

The fabrication of new functional submicron and nanoscale devices with chemical or true three-dimensional patterns requires new complementary soft-lithography approaches. Polymers come naturally as ideal "inks" or building blocks for soft lithography because of their defined architecture, wide range of chemical functionalities that can be incorporated, and ease of processing on micro and nano scales. Optical systems, and microelectronic devices such as transistors and light-emitting diodes, have been realized with polymers and soft lithography. Among the most promising polymer-based microfabrication strategies are nanoimprint lithography, microcontact printing, micro-fluid-contact printing, lift-up, micromolding in capillaries, replica molding, solvent-assisted micromolding, and its variations (for references see [5]). Polymer patterns can also be formed on chemically heterogeneous surfaces prepared by microcontact printing of self-assembled monolayers and by performing photolithography in the optical near field of an elastomeric mask. However, one of the drawbacks is that most polymers possess poor etch resistivity. Thus, the choice of macromolecular "inks" that can be shaped or transferred with the stamp, to a silicon wafer, for example, and used as a "single-step" resist is rather limited. Poly(ferrocenylsilane)s constitute a group of polymers that combine both macromolecular properties and etch resistivity and are ideal materials for one-step resists. This section describes the fabrication of microstructures of poly(ferrocenylmethylphenylsilane) (PFMPS) and their use as etch resist. The asymmetrically substituted PFS was selected, as symmetrically substituted polymers (such as poly(ferrocenyldimethylsilane)) crystallize, giving heterogeneous, semicrystalline films. Clearly, for homopolymer etch resist applications, structurally homogeneous films are needed. Two soft lithography approaches for pattern formation are presented. One employs solvent-assisted polymer dewetting, and the other relies on the concept of capillary force lithography.

### 3.1 Printing of Organometallic Polymers by Soft Lithography

The printing of etch-resistant polymers by soft lithography methods is an attractive option for the fabrication of lithographic masks. Microcontact printing is a versatile technique to generate chemically distinct patterns on solid

substrates. An elastomer stamp, usually made from poly(dimethylsiloxane) (PDMS), is used to transfer the "ink" to the surface of the substrate by contact printing [61]. Usually, small molecules are employed as inks that upon contact will react with the substrate. When the stamp is removed, a pattern of ink molecules, dictated by the stamp, remains on the surface of the substrate. Recently, approaches where the ink consists of a macromolecule have been attracting attention [62, 63].

The limited use of macromolecular inks can be attributed to poor wetting characteristics of PDMS surfaces by many polymers. Stamps prepared from PDMS have a very low surface tension (around 20 mN/m), compared to common polymers [64]. This is why attempts to use poly(ferrocenyldimethylsilane) as an ink in classical microcontact printing ($\mu$CP) were not successful. Wettability of the PDMS stamps used for $\mu$CP can be improved by treating the stamp with an oxygen plasma prior to inking. Exposure to an $O_2$-based plasma oxidizes the surface of the stamp and increases the surface free energy of PDMS [65]. However, the thin silica-like layer that is formed during plasma treatment [66] thermally expands and generates mechanical stress on the stamp upon cooling. The relaxation of this stress induces buckling of the brittle surface layer, and a periodic wavy structure with an orientation perpendicular to the pattern of the stamp is introduced [67]. This fine structure can also be replicated by the PFS used as an ink, and a pattern on two independent length scales is formed (Fig. 5) [68, 69].

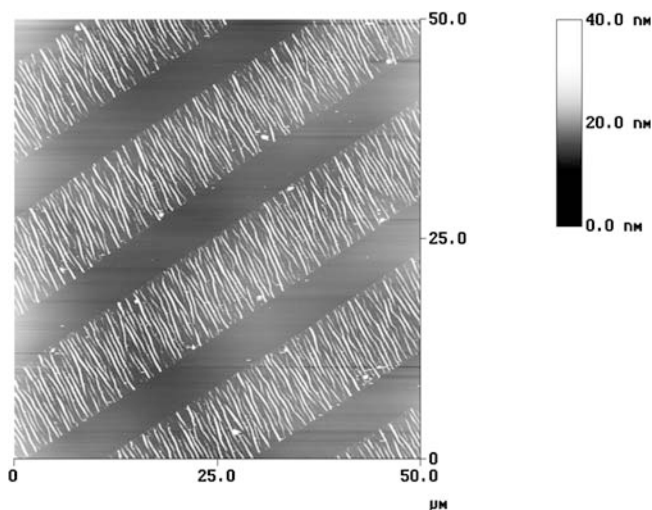


**Fig. 5** AFM image of a poly(ferrocenyldimethylsilane) pattern printed with an oxygen-plasma-treated PDMS stamp. The corrugated structure is a result of the stress generated by the difference in thermal expansion between the PDMS matrix and the oxidized surface. Reprinted with permission from [69]. Copyright 2004, John Wiley & Sons, Inc.

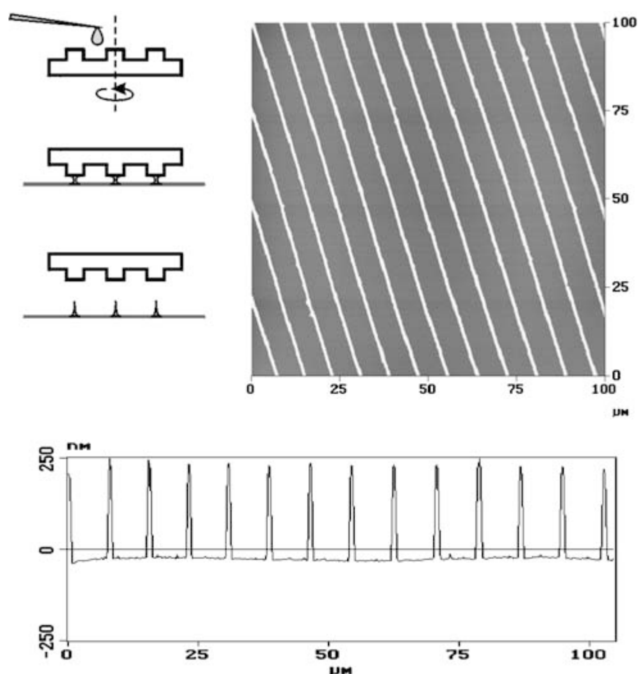


**Fig. 6** Solvent-assisted dewetting of poly(ferrocenylmethylphenylsilane) (PFMPS) confined between a PDMS stamp and silicon substrate. Schematic diagram (*left*) and AFM height image (*right*) with section analysis after 10 minutes of $CF_4/O_2$-RIE treatment. Reprinted with permission from [5]. Copyright 2003, American Chemical Society

When using less aggressive cleaning and oxidation techniques, it is also possible to eliminate the corrugation formation. Cleaning the PDMS stamp in a mild ozone/UV environment will still render the PDMS surface hydrophilic [70], but will not result in extensive surface heating and therefore thermal-expansion-related stress. Patterns revealed after using these stamps have a spacing that corresponds to the periodicity of the stamp structures. This suggests that during printing, the polymer solution dewets between the stamp and Si surface, forming continuous lines in the middle of the protruding stamp contact areas (Fig. 6). Similar results were observed by Braun and co-workers using a hexagonally structured stamp [71]. As shown in Fig. 6, these lines with a width on the order of 1 µm can be etched into the underlying silicon substrate.

## 3.2
## Directed Dewetting

A chemically patterned substrate, obtained by microcontact printing, may serve as a template that directs the adsorption of macromolecules, as is demonstrated in Fig. 7. A 1*H*,1*H*,2*H*,2*H*-perfluorodecyltrichlorosilane self-

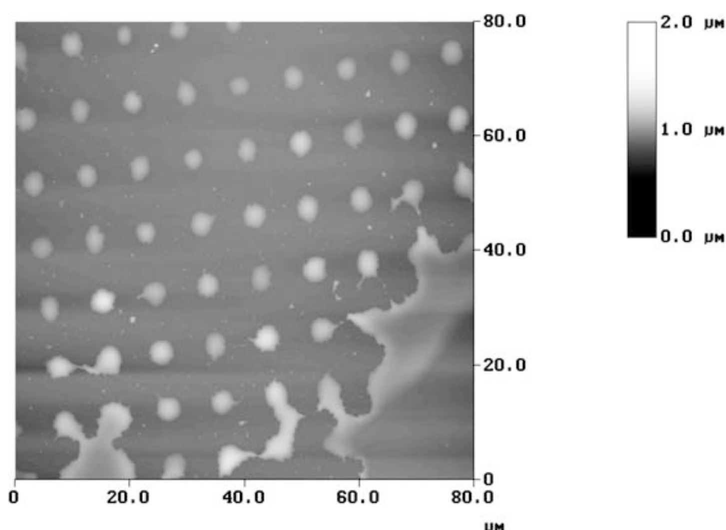


**Fig. 7** AFM image of a microcontact printed silicon substrate, partially dewetted by a poly(ferrocenyldimethylsilane) film. The circular features, corresponding to bare silicon, are wetted by PFS. Reprinted with permission from [69]. Copyright 2004, John Wiley & Sons, Inc.

assembled monolayer was printed on a silicon substrate. The circular regions correspond to bare silicon. Poly(ferrocenyldimethylsilane) was then spin-coated onto this hydrophylically/hydrophobically patterned substrate, which directed the dewetting of the polymer film. PFS preferentially wetted the bare silicon circles.

## 3.3 Capillary Force Lithography

The principles of capillary force lithography [72, 73] and a representative pattern of poly(ferrocenylmethylphenylsilane) (PFMPS) stripes on Si obtained by this technique, are shown in Fig. 8. A PDMS mold was placed in contact with a thin PFMPS film (thickness 27 nm) and, subsequently, the temperature was raised above the $T_g$ (74 °C) of the polymer. The polymer, initially confined in a thin film, is squeezed out from areas of contact between stamp and substrate. It diffuses into the grooves where structures are formed along the vertical walls of the stamp due to capillary rise. Polymer structures, which are approximately 110 nm high and 500 nm wide, were fabricated. Section analysis of the AFM height images revealed a meniscus of the capillary rise (note the different scales for the vertical and horizontal directions). The structures were developed by $CF_4/O_2$-RIE. After resist removal, a patterned substrate as shown earlier in Fig. 2 was obtained.

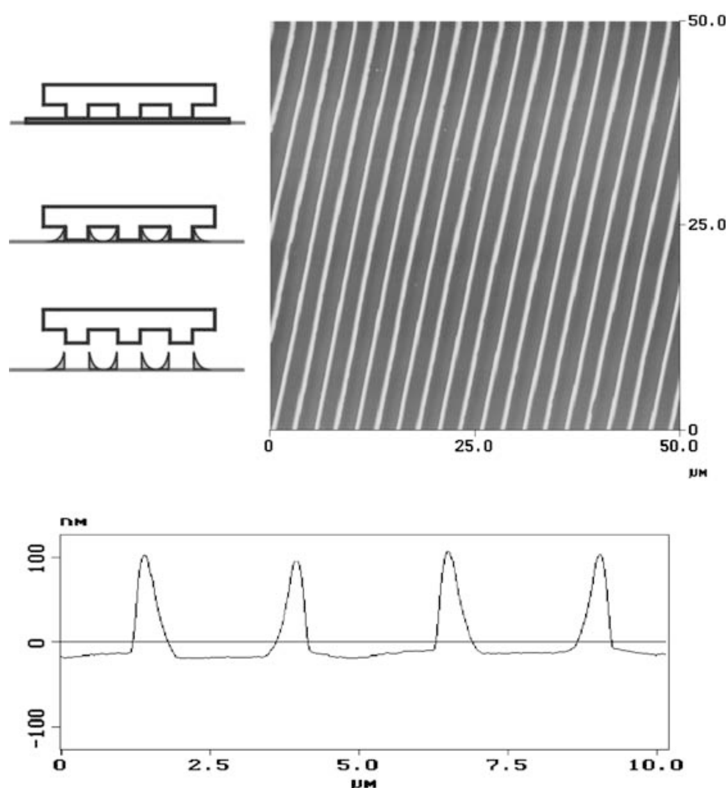


**Fig. 8** Capillary force lithography of a thin PFMPS film with a $2 \times 3\,\mu m$ PDMS stamp. Schematic diagram (*left*) and AFM height image with section analysis. The height of the resulting features is 110 nm and the initial thin film thickness was 27 nm. Reprinted with permission from [5]. Copyright 2003, American Chemical Society

Very thin polymer films do not provide enough material to fill the grooves of the stamp completely. As a result, two polymeric lines are formed per groove. This is clearly seen in AFM profiles and was also confirmed by SEM. Increasing the thickness of the initial polymer film results in thicker double lines, which eventually merge when the film thickness exceeds approximately 140 nm. This allows one to tune the lateral dimensions of the polymer lines (Fig. 9).

Figure 10 displays profiles of microstructures obtained with PFMPS before and after etching, showing that approximately 300 nm of silicon was removed in a 10 min treatment. The remaining resist (polymer with oxide layer) still present at the top of the silicon structures can easily be stripped in $HNO_3$.

Soft lithography-based approaches are versatile and cost-effective methods to generate patterns on the micrometer lengthscale. Submicrometer structures are also accessible provided that PDMS stamps with corresponding geometries are available.

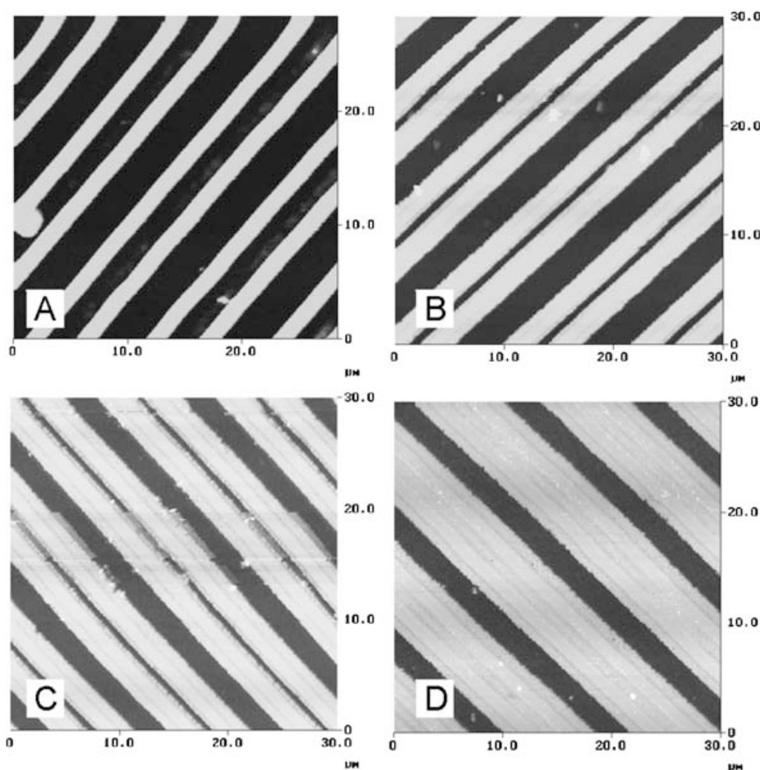


**Fig. 9** Patterns in silicon after etching ($CF_4/O_2$-RIE) and resist stripping. The initial polymer film thickness was **A** 30 nm, **B** 80 nm, **C** 100 nm, and **D** 150 nm. Reprinted with permission from [5]. Copyright 2003, American Chemical Society

## 4 Lithographic Applications of Poly(ferrocenylsilane) Block Copolymers

Issues regarding the self-assembly of organic–organometallic block copolymers in thin films and applications of the resulting nanoperiodic patterns are discussed in this section.

### 4.1 Structure Formation via Block Copolymer Self-Assembly

The self-organization of block copolymers constitutes a versatile means of producing ordered periodic structures with phase-separated microdomain sizes on the order of tens of nanometers. The morphology of microdomains formed by diblock copolymers in the bulk has been intensively researched and is by now a relatively well-understood area [74, 75].

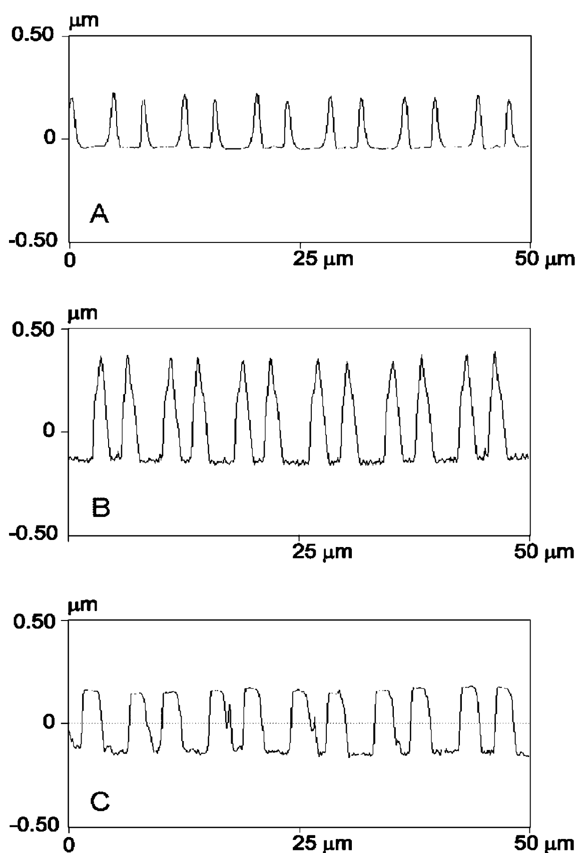


**Fig. 10** Pattern development in capillary force lithography ($3 \times 5\,\mu m$ stamp) with poly(ferrocenylmethylphenylsilane). AFM section analysis of: **A** PFS mask, **B** structures after etching ($CF_4/O_2$-RIE, 10 min), **C** Si structures after removal of the resist in $HNO_3$. Reprinted with permission from [5]. Copyright 2003, American Chemical Society

In neat diblocks, three "classical" ordered microphases are usually distinguished (Fig. 11). These include alternating lamellae, hexagonally packed cylinders, and body-centered-cubic packed spheres. In addition, some other, more complex microstructures may appear, especially near the order–disorder transition.

A series of styrene-ferrocenyldimethylsilane block copolymers form periodic structures on a lengthscale comparable to the size of the polymers [6] (Fig. 12). Pure diblock copolymers phase-separate into an equilibrium structure that depends on the corresponding $\chi$-parameter [77], the length of the block copolymer, and the volume fraction of the two phases. Knowledge of the $\chi$-parameter will allow one to target a specific morphology by adjusting the molar mass and composition of the diblock copolymer accordingly (Scheme 2).

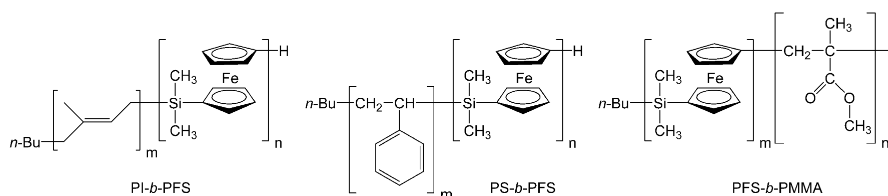


**Scheme 2** Examples of organic-ferrocenylsilane block copolymers

**Fig. 11** The classical morphologies in block copolymer systems

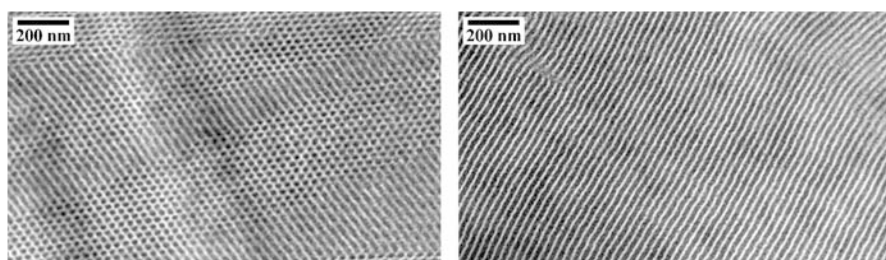


**Fig. 12** Bright-field TEM micrograph of a cylinder-forming and a lamellar-forming PS-*b*-PFS diblock copolymer. Reproduced with permission from [6]. Copyright 1999, Wiley Periodicals, Inc., A Wiley Company

## 4.2
## Block Copolymer Thin Films

In thin films, the presence of a substrate and surface can induce orientation of the structure and can result in changes in domain dimensions or in phase transitions due to preferential segregation of one of the blocks at the substrate or the surface. If one block has a higher affinity for the substrate, it will exhibit preferential wetting, resulting in an orientation of the phase-separated domains parallel to the substrate [78]. Similar wetting will occur at the free surface, i.e., the block with the lower surface free energy will enrich the surface. In relatively thick block copolymer films, a mismatch between the film thickness and the bulk lattice spacing can be distributed over many layers. As the film thickness is decreased to a value equal to a few domain periods, the frustration due to the mismatch becomes more significant and can be released by the formation of islands or holes [79] (Fig. 13).

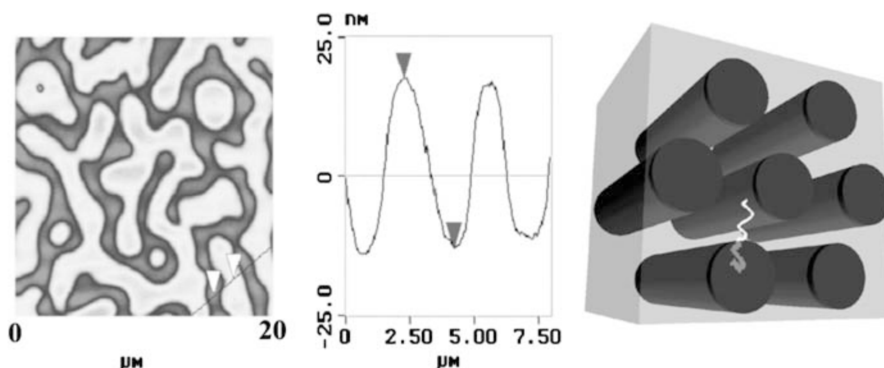


**Fig. 13** Representation of a cylinder-forming (PS-*b*-PFS) block copolymer (*right*). When confined in a thin film with a thickness of 2× the lattice spacing, islands and holes are formed (*left*) due to an incommensurate film thickness

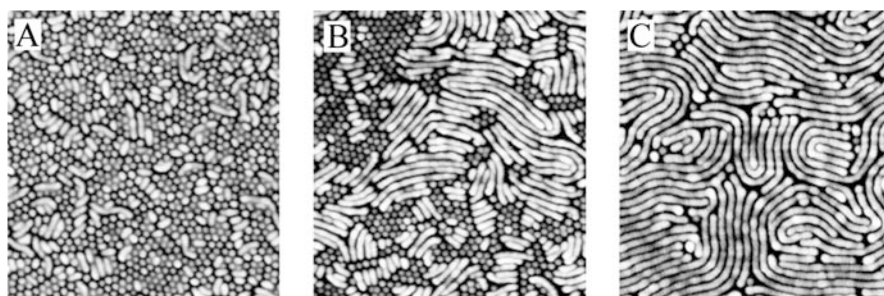


**Fig. 14** Tapping mode AFM height images of PS-*b*-PFS block copolymer thin films of different initial thickness: **A** 30 nm, **B** 35 nm, **C** 40 nm. Each scan size is 1 $\mu m^2$. The organic matrix phase was selectively removed prior to AFM imaging by means of an $O_2$-RIE treatment. Reprinted with permission from [80]. Copyright 2001, American Chemical Society

Film thickness constraints can also be exploited to control the orientation of the nanodomains. More specifically, when the thickness of the film approaches the lattice constant of the block copolymer, the orientation of the nanodomains is sometimes altered with respect to the substrate. Simply stated, the stress generated by the incommensurate film thickness can be relieved by a change in domain orientation. This is further illustrated by an example in Fig. 14. A styrene-ferrocenyldimethylsilane block copolymer (PS-*b*-PFS), consisting of a styrene fraction of 0.73 forms a cylindrical structure in the bulk [6]. Within a thin film, the pattern that is formed by the block copolymer also depends on the film thickness [80].

Alternatively, the morphology of a thin diblock film can be altered by a subtle change in composition. It was demonstrated for a series of isoprene-ferrocenyldimethylsilane block copolymers (PI-*b*-PFS) that the structure

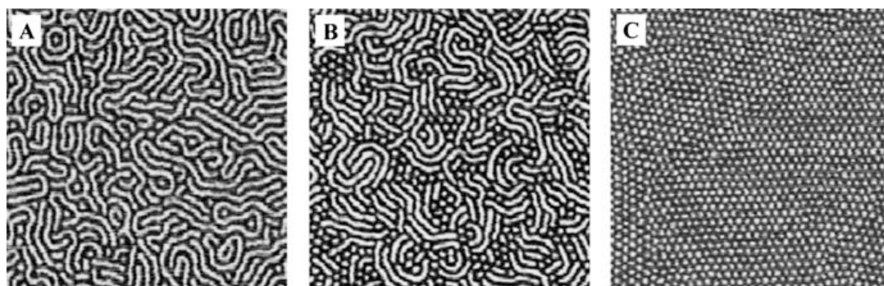


**Fig. 15** Tapping mode AFM images of 30 nm thin PI-*b*-PFS copolymer films of different compositions: **A** PI volume fraction of 0.72, **B** PI fraction of 0.76, **C** PI fraction of 0.80. Each scan size is 1 $\mu m^2$. Reprinted with permission from [81]. Copyright 2000, American Chemical Society

within a 30 nm thin film could be significantly changed by a slight compositional difference, although the bulk structures all had the same morphology [81]. This is demonstrated in Fig. 15.

## 4.3 Self-Assembling Resists

Block copolymers can be employed as templates to direct the deposition of inorganic nanostructures. Park et al. [82] used an $OsO_4$-stained microphase-separated thin film of poly(styrene-*block*-butadiene) that produced holes upon RIE in silicon nitride substrates. The etch ratio between the two phases, stained butadiene and styrene, was only about 1 : 2. Möller et al. discussed the use of poly(styrene-*block*-2-vinylpyridine), to prepare masks for nanolithography by loading the PVP domains with gold particles [83] or by selective growth of Ti on top of the PS domains [84].

Thin films of organic–organometallic block copolymers self-assemble to form lateral regions that have a significantly different etching behavior. Furthermore, the two phases already contain all the elements necessary to generate large etching contrast, without the need for staining or loading. The organometallic-rich areas enclose regions of high resistance against removal by oxygen and fluorocarbon plasmas, whereas the organic rich phase is quickly removed. This opens up the possibility of transferring the pattern generated by block copolymer self-assembly in a one-step etching process onto the underlying substrate [7].

A nanostructured silicon surface obtained after etching, as measured via AFM, is shown in Fig. 16. The organic constituents of the block copolymer have been selectively removed by the action of the oxygen plasma, leaving the oxidized metal-containing phase behind. Such self-assembling nanolithographic templates were recently employed to obtain high-density magnetic arrays in cobalt substrates (Fig. 17) [8].

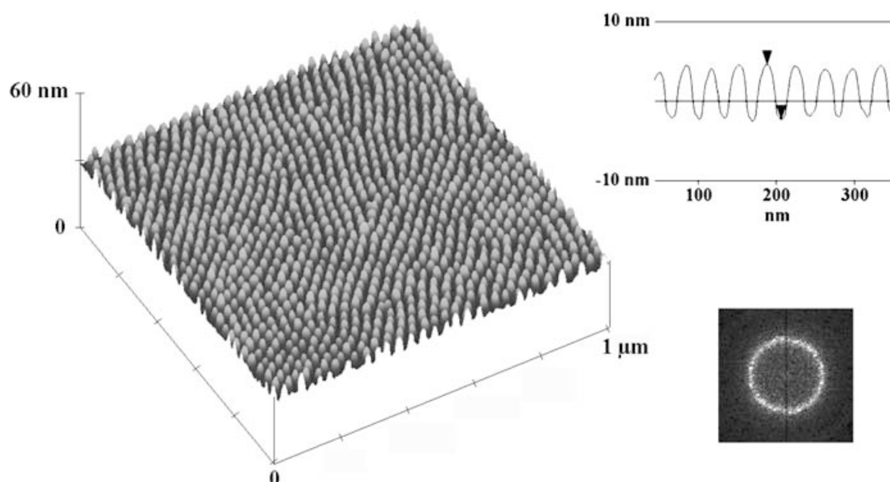


**Fig. 16** Tapping mode AFM height image of an etched PI-*b*-PFS organic–organometallic diblock copolymer film. The dots are a result of the block copolymer phase separation. Reprinted with permission from [7]. Copyright 2000, American Chemical Society

Patterns resulting from block copolymer phase separation show good short-range order but usually lack long-range order, which could limit their use in some applications. Combining block copolymer self-assembly with long-range ordering methods would allow nanostructures to be fabricated in precise positions on a substrate. Graphoepitaxy is a method that allows ordered arrays of nanostructures to be formed by spin casting a block copolymer over surfaces patterned with shallow grooves [85]. Figure 18 shows a remarkably well-ordered pattern obtained by spin-coating a PS-*b*-PFS block copolymer on the appropriately structured silicon wafer [86]. It also shows how the long-range order of the pattern changes with the width of the grooves. Within a 500-nm-wide groove, about three rows of close-packed PFS features are aligned parallel to the sidewall (Fig. 18a). In the 320 nm grooves, some regions show a close-packed pattern extending across the groove, but there is a significant number of defects in the pattern (Fig. 18b). However, the alignment is nearly perfect in 240-nm-wide grooves, in which the groove width is comparable to the typical polymer grain size. The features have a sixfold symmetry, and the superposed fast Fourier transforms of the images of several grooves (Fig. 18c) show that the pattern in each groove has the same orientation. The rare domain-packing defects are apparently generated from the edge roughness of the grooves. The ordered block copolymer domain patterns are then transferred into an underlying silica film using a single etching step to create a well-ordered hierarchical structure consisting of arrays of silica pillars with 20 nm feature sizes and aspect ratios greater than 3.

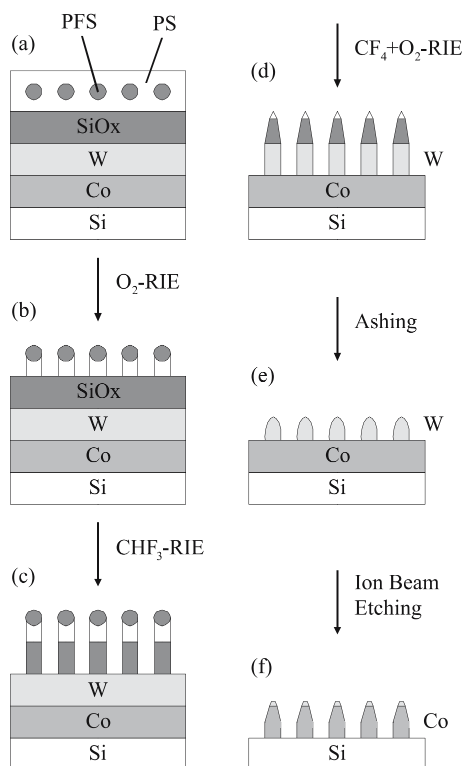


**Fig. 17** Fabrication process of cobalt dot arrays via block copolymer lithography. **A** A block copolymer thin film on a multilayer of silica, tungsten, and cobalt. **B** The block copolymer lithographic mask is formed through a $O_2$-RIE process. The PFS domains are partly oxidized. **C** The silica film is patterned using $CHF_3$-RIE. **D** The tungsten hard mask is patterned using $CF_4/O_2$-RIE. **E** Removal of silica and residual polymer by high-pressure $CHF_3$-RIE. **F** The cobalt dot array is formed using ion beam etching. Reproduced with permission from [8]. Copyright 2001, Wiley-VCH Verlag GmbH

## 5 Guided Deposition of Poly(ferrocenylsilane) Polyions

Water-soluble poly(ferrocenylsilane) polycations, belonging to the rare class of main chain organometallic polyelectrolytes, have been reported by us and others [35, 36, 87, 88]. These compounds are of interest because they combine the unusual properties of poly(ferrocenylsilane)s with the processability of polyelectrolyte solutions—for example, enabling one to make use of ionic interactions to deposit these polymers onto substrates. Polyelectrolytes can be employed in layer-by-layer self-assembly processes to form ultrathin multilayer films with controlled thickness and composition [89, 90].

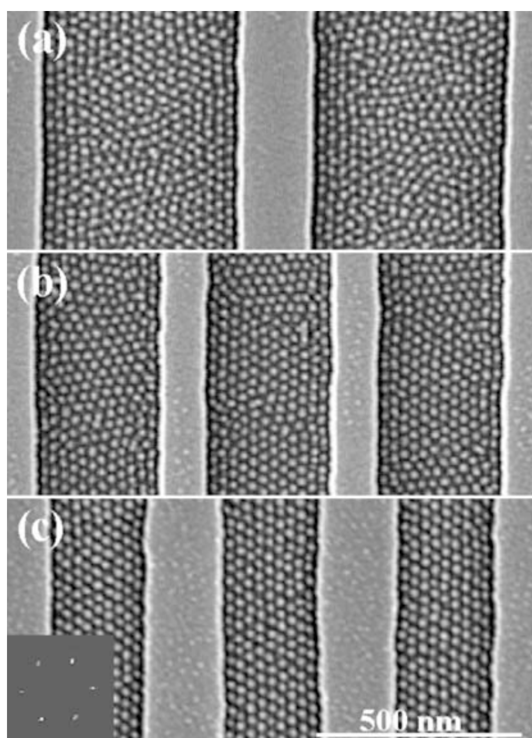


**Fig. 18** Scanning electron micrographs of annealed (48 h) and plasma-treated PS-*b*-PFS films spun at 3500 rpm on silica gratings with **A** 500-nm-wide grooves; **B** 320-nm-wide grooves; **C** 240-nm-wide grooves. The inset is the Fourier transform of the plan-view pattern showing sixfold symmetry. Reprinted with permission from [86]. Copyright 2002, American Institute of Physics

The incorporation of metals in multilayer thin films significantly extends the scope of useful characteristics associated with these films. By employing, for instance, polymeric Ru(II) complexes as polycationic species and poly(sodium acrylate) as polyanions in the layer-by-layer deposition process, efficient light-emitting solid-state devices could be fabricated [91]. In another example, a ferrocene-containing redox-active polycation was combined with an enzyme to produce electrocatalytically active enzyme/mediator multilayer structures [92]. Multilayers composed of poly(4-vinylpyridine) complexed with $[Os(bpy)_2Cl]^{+/2+}$ and poly(sodium 4-styrenesulfonate), for example, were used to accomplish the electrocatalytic reduction of nitrite [93].

Although cationic poly(ferrocenylsilane)s have been used in combination with commercially available organic polyanions to fabricate heterostructured multilayer films [36, 37], fully organometallic multilayers were not reported until recently due to the lack of availability of anionic organometallic polyions [94, 95]. Multilayer structures composed of poly(ferrocenylsilane)

polyanions and polycations are of interest as redox-active thin films. Besides forming continuous organometallic multilayer thin films, we explored the layer-by-layer deposition of poly(ferrocenylsilane) polyions onto, for example, hydrophilically/hydrophobically modified substrates, with the aim of building two-dimensionally patterned organometallic multilayers. In general, surfaces modified with microscopically patterned conducting [96], luminescent [97], or redox-active polymer [98] films have potential use in microelectronic and optoelectronic devices and microsensor arrays. Patterned organometallic multilayers may be useful as etch barriers in reactive ion etch processes [4].

The synthesis of PFS polyions was described in detail elsewhere [32, 33, 36]. We employ a poly(ferrocenylsilane) featuring chloropropylmethylsilane repeat units as an organometallic main chain that already has reactive pendant groups in place for further functionalization (Scheme 3). Poly(ferrocenyl(3-chloropropyl)methylsilane) was readily accessible by transition-metal catalyzed ring-opening polymerization [22, 23] of the corresponding (3-chloropropyl)methylsilyl[1]ferrocenophane [36]. By means of halogen exchange, poly(ferrocenyl(3-chloropropyl)methylsilane) can be con-

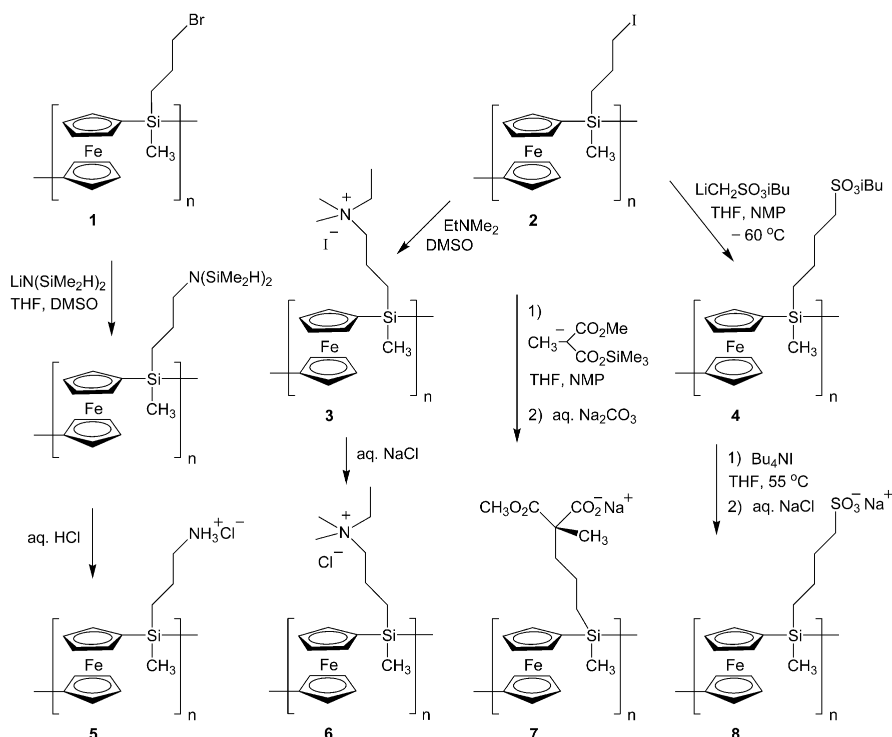


**Scheme 3** Examples of poly(ferrocenylsilane) polycations and polyanions

verted quantitatively into its bromopropyl (**1**) or iodopropyl (**2**) analogues, which are particularly suitable for functionalization by nucleophilic substitution. Ionic functionalities were introduced by side-group modification of **1** and **2**. Scheme 3 shows examples of weak and strong PFS polyelectrolytes.

UV/Vis absorption spectroscopy was used to monitor the electrostatic self-assembly of the organometallic polyions **5/7** and **6/8**. The increase in absorption at $\lambda_{max} = 216$ nm shows a linear dependence on the number of bilayers deposited on quartz slides. Information on the increase of film thickness with the number of bilayers was obtained from spectroscopic ellipsometry [92]. Thickness measurements on the films, built up on silicon wafers, were carried out after each bilayer deposition. The fitted multilayer thickness increased linearly with the number of deposited bilayers, in accordance with the UV/Vis absorption spectroscopy results. For the strong polyions **6** and **8**, deposited under salt-free conditions, a thickness contribution of 0.6 nm per bilayer was found. In the presence of NaCl, markedly thicker multilayers were obtained (4.5 nm/bilayer).

Poly(ferrocenylsilane)s are redox-active materials, showing fully reversible electrochemical oxidation and reduction [27–29]. A typical voltammogram shows two oxidation waves, indicating intermetallic coupling between neighboring iron centers in the polymer chain. The first oxidation wave was attributed to oxidation of ferrocene centers having neutral neighboring units. In the second wave, at higher potentials, oxidation of the remaining ferrocene centers, predominantly in positions next to oxidized units, is completed [99–101]. Thus, the charge ratio between the two oxidation peaks is approximately 1 : 1. The redox behavior of the multilayer thin films, fabricated on gold electrodes, was studied. Stable multilayers were obtained by first adsorbing a sodium 3-mercapto-1-propanesulfonate monolayer on Au, producing a negatively charged surface ideally suited for polyion adsorption [92]. Cyclic voltammograms of multilayer thin films of polyions **5/7** were recorded for samples having an increasing number of bilayers (1–7) to monitor the electrochemical response as the surface concentration of redox sites increased. The CVs of thin films composed of 1, 3, and 6 bilayers (Fig. 19) show the two oxidation and reduction waves typical of poly(ferrocenylsilane)s. Integration of the voltammetric peaks allows one to calculate the charge involved in the redox processes. From this the surface coverage $\Gamma$ of ferrocene units can be obtained, using the relation $\Gamma = Q/n \cdot F \cdot A$, where $Q$ is the charge, $n$ is the number of exchanged electrons ($n = 1$ in this case), $F$ is Faraday's constant (96 485 C $mol^{-1}$), and $A$ is the electrode surface area employed in the measurements (0.44 $cm^2$) [102, 103]. Using this relation, one organometallic bilayer of polyions **5/7**, deposited under salt-free conditions, was found to correspond to a ferrocene surface coverage of 0.45 ferrocene units/$nm^2$. The surface coverage $\Gamma$ (ferrocene units/$nm^2$) increased linearly with the number of bilayers.

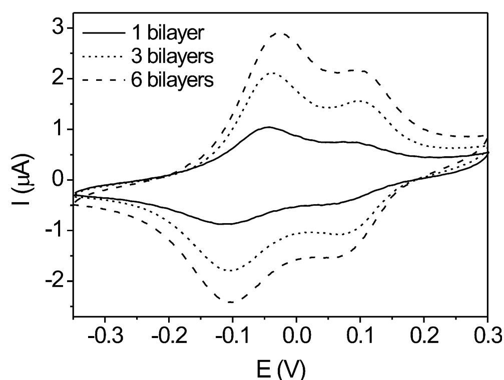


**Fig. 19** Cyclic voltammogram of 1, 3, and 6 organometallic bilayers (**5**/**7**) deposited on a gold electrode featuring a monolayer of sodium 3-mercapto-1-propanesulfonate taken at a scan rate of $\nu = 30\,\mathrm{mV/s}$. Reprinted with permission from [94]. Copyright 2002, American Chemical Society

In addition to producing continuous fully organometallic multilayer thin films, one can form patterned organometallic multilayer structures by confining the deposition of the poly(ferrocenylsilane) polyelectrolytes to selected areas on substrates, which broadens the applicability of such multilayers [104]. The selective deposition of polyelectrolytes on hydrophilically/ hydrophobically patterned gold substrates has been described [105, 106]. In this case, patterned self-assembled monolayers consisting of, for example, methyl-terminated and oligo(ethylene glycol)-terminated alkanethiols were introduced on gold substrates using microcontact printing [57–59]. Areas covered with oligo(ethylene glycol)-terminated alkanethiols were found to prevent adsorption of polyelectrolytes. Here, as a demonstration, a gold substrate was patterned with 5 μm-wide methyl-terminated alkanethiol lines, separated by 3 μm, by microcontact printing of 1-octadecanethiol. The uncovered areas were subsequently filled in with 11-mercapto-1-undecanol, resulting in a hydrophilically/hydrophobically patterned substrate. AFM height and friction force images of these patterned self-assembled monolayers (Fig. 20, top images) show minimal height contrast but a large contrast in friction force, with the hydroxyl-terminated lines corresponding to the high-friction areas. The patterned substrate was then coated with 12 bilayers of polyions **5**/**7** and again examined by contact mode AFM. Clearly, after deposition, the height contrast increased, and the contrast in friction force was reversed, which shows that the multilayers grow selectively on the broad, methyl-terminated stripes (Fig. 20, lower images) [94].

The resistivity of the hydroxyl-terminated areas to polyion deposition was demonstrated by first forming a monolayer of 11-mercapto-1-undecanol on a gold substrate, which was then processed in a similar manner as the patterned substrates, and subsequently analyzed by XPS. Fe 2p signals, in-

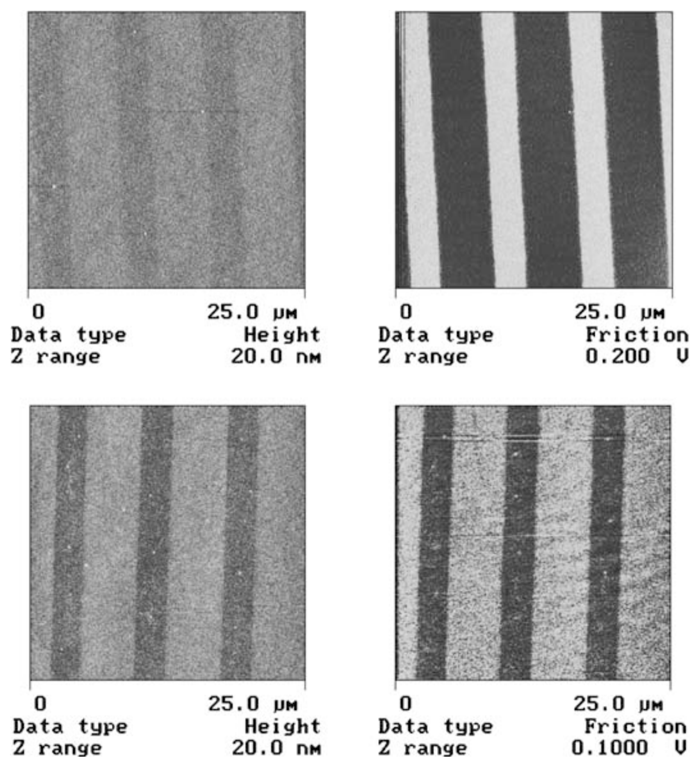


**Fig. 20** Multilayer deposition on a hydrophilically/hydrophobically patterned gold substrate. Upper AFM images: height (*left*) and friction force (*right*) images of patterned methyl- and hydroxyl- alkanethiol self-assembled monolayers. Adsorption of poly(ferrocenylsilane) polyions (**5**/**7**, 12 bilayers) occurs selectively on the broad methyl-terminated stripes (lower AFM images). Reprinted with permission from [94]. Copyright 2002, American Chemical Society

dicating adsorbed polyions, were absent in the survey scan. The selective adsorption of the polyions on the methyl-terminated regions of the surface is most likely driven by favorable hydrophobic interactions [107] between these areas and the hydrophobic poly(ferrocenylsilane) backbone, minimizing the interfacial free energy of the system. Such favorable secondary interactions with the hydrophilic regions, which are hydrated under the processing conditions [108], are excluded.

## 6 Conclusions

Metal-containing polymers appear to be valuable candidates for developing highly etch-resistant resists. Masking layers with a high etch resistance are

potentially useful for very thin resist layer applications, since reducing resist film thickness is a viable method to prevent pattern collapse when fabricating high-aspect-ratio structures.

Advances in printing techniques of polymers may also contribute to the progress in cost-effective pattern replication procedures. The ability to replicate and print polymer patterns on micron and submicron lengthscales opens up a route to economically fabricate etch-resistant patterns for applications where metallic contaminations are not relevant. Examples of such applications include the fabrication of photomasks, microfluidic devices, optical components, data storage arrays, etc.

Self-assembly of organometallic block copolymers provides access to nanolithographic masks. A broad range of nanoscale morphologies, which can be developed in one step using reactive ion etching, is available. These patterns can be confined on a surface, and their long-range order can be further improved using techniques such as graphoepitaxy [109].

Poly(ferrocenylsilane) polyions are readily processed to novel, fully organometallic multilayer thin films. Furthermore, these organometallic polyions, featuring a hydrophobic backbone, enable one to make use of both electrostatic and hydrophobic interactions to fabricate self-organized patterns on templated substrates, with potential applications as aqueous processable ultrathin etch resists.

**Acknowledgements** This work was supported in part by the European Community's Human Potential Programme under contract HPRN-CT-1999-00151, [PolyNano].

## References

1. Abd-El-Aziz AS (2004) Overview of organoiron polymers. In: Abd-El-Aziz AS, Carraher CE, Pittman CU, Sheats JE, Zeldin M (eds) Macromolecules containing metal and metal-like elements, vol 2. Wiley, New York, p 1–27
2. Abd-El-Aziz AS (2002) Macromol Rapid Commun 23:995
3. Manners I (2004) Synthetic metal-containing polymers. Wiley, New York
4. Lammertink RGH, Hempenius MA, Chan VZH, Thomas EL, Vancso GJ (2001) Chem Mater 13:429
5. Korczagin I, Golze S, Hempenius MA, Vancso GJ (2003) Chem Mater 15:3663
6. Lammertink RGH, Hempenius MA, Thomas EL, Vancso GJ (1999) J Polym Sci Part B: Polym Phys 37:1009
7. Lammertink RGH, Hempenius MA, van den Enk JE, Chan VZH, Thomas EL, Vancso GJ (2000) Adv Mater 12:98
8. Cheng JY, Ross CA, Chan VZH, Thomas EL, Lammertink RGH, Vancso GJ (2001) Adv Mater 13:1174
9. Hinderling C, Keles Y, Stöckli T, Knapp HF, de los Arcos T, Oelhafen P, Korczagin I, Hempenius MA, Vancso GJ, Pugin R, Heinzelmann H (2004) Adv Mater 16:876
10. Lastella S, Jung YJ, Yang HC, Vajtai R, Ajayan PM, Ryu CY, Rider DA, Manners I (2004) J Mater Chem 14:1791
11. Nguyen MT, Diaz AF, Dementev VV, Pannell KH (1993) Chem Mater 5:1389

12. Péter M, Hempenius MA, Lammertink RGH, Vancso GJ (2001) Macromol Symp 167, 285
13. Péter M, Hempenius MA, Kooij ES, Jenkins TA, Roser SJ, Knoll W, Vancso GJ (2004) Langmuir 20:891
14. Zou S, Ma Y, Hempenius MA, Schönherr H, Vancso GJ (2004) Langmuir 20:6278
15. Arsenault AC, Míguez H, Kitaev V, Ozin GA, Manners I (2003) Adv Mater 15:503
16. MacLachlan MJ, Ginzburg M, Coombs N, Coyle TW, Raju NP, Greedan JE, Ozin GA, Manners I (2000) Science 287:1460
17. Massey J, Power KN, Manners I, Winnik MA (1998) J Am Chem Soc 120:9533
18. Cao L, Massey JA, Winnik MA, Manners I, Riethmuller S, Banhart F, Spatz JP, Möller M (2003) Adv Funct Mater 13:271
19. Rosenberg H, Rausch MD (1962) US Patent 3 060 215
20. Foucher DA, Tang BZ, Manners I (1992) J Am Chem Soc 114:6246
21. Rulkens R, Lough AJ, Manners I (1994) J Am Chem Soc 116:797
22. Ni YZ, Rulkens R, Pudelski JK, Manners I (1995) Macromol Rapid Commun 16:637
23. Gómez-Elipe P, Macdonald PM, Manners I (1997) Angew Chem Int Ed 36:762
24. Rasburn J, Petersen R, Jahr T, Rulkens R, Manners I, Vancso GJ (1995) Chem Mater 7:871
25. Foucher D, Ziembinski R, Petersen R, Pudelski J, Edwards M, Ni YZ, Massey J, Jaeger CR, Vancso GJ, Manners I (1994) Macromolecules 27:3992
26. Foucher DA, Ziembinski R, Tang BZ, Macdonald PM, Massey J, Jaeger CR, Vancso GJ, Manners I (1993) Macromolecules 26:2878
27. Manners I (2003) Macromol Symp 196:57
28. Kulbaba K, Manners I (2001) Macromol Rapid Commun 22:711
29. Manners I (1999) Chem Commun 857
30. Nelson JM, Rengel H, Manners I (1993) J Am Chem Soc 115:7035
31. Nelson JM, Lough AJ, Manners I (1994) Angew Chem Int Ed 33:989
32. Hempenius MA, Vancso GJ (2002) Macromolecules 35:2445
33. Hempenius MA, Brito FF, Vancso GJ (2003) Macromolecules 36:6683
34. Wang Z, Lough A, Manners I (2002) Macromolecules 35:7669
35. Power-Billard KN, Manners I (2000) Macromolecules 33:26
36. Hempenius MA, Robins NS, Lammertink RGH, Vancso GJ (2001) Macromol Rapid Commun 22:30
37. Ginzburg M, Galloro J, Jäkle F, Power-Billard KN, Yang S, Sokolov I, Lam CNC, Neumann AW, Manners I, Ozin GA (2000) Langmuir 16:9609
38. Ni YZ, Rulkens R, Manners I (1996) J Am Chem Soc 118:4102
39. Lammertink RGH, Hempenius MA, Vancso GJ (2000) Langmuir 16:6245
40. Rulkens R, Ni YZ, Manners I (1994) J Am Chem Soc 116:12121
41. Resendes R, Massey J, Dorn H, Winnik MA, Manners I (2000) Macromolecules 33:8
42. Wang XS, Winnik MA, Manners I (2002) Macromolecules 35:9146
43. Wang XS, Winnik MA, Manners I (2002) Macromol Rapid Commun 23:210
44. Korczagin I, Hempenius MA, Vancso GJ (2004) Macromolecules 37:1686
45. Kloninger C, Rehahn M (2004) Macromolecules 37:1720
46. d'Agostino R (1990) Plasma Deposition, Treatment, and Etching of Polymers. Academic Press, New York
47. Manos DM, Flamm DL (1988) Plasma etching: an introduction. Academic Press, New York
48. van Roosmalen AJ, Baggerman JAG, Brader SJH (1991) Dry etching for VSLI. Plenum, New York
49. Flamm DL, Donnelly VM (1981) Plasma Chem Plasma Proc 1:317

50. Knizikevicius R, Galdikas A, Grigonis A (2002) Vacuum 66:39
51. Kokkoris G, Gogolides E, Boudouvis AG (2002) J Appl Phys 91:2697
52. Jansen H, Gardeniers H, de Boer M, Elwenspoek M, Fluitman J (1996) J Micromech Microeng 6:14
53. Oehrlein GS, Williams HR (1987) J Appl Phys 62:662
54. Coburn JW, Kay E (1979) Solid State Technol 22:117
55. Strobel M, Corn S, Lyons CS, Korba GA (1987) J Polym Sci A 25:1295
56. Strobel M, Thomas PA, Lyons CS (1987) J Polym Sci A 25:3343
57. Mogab CJ, Adams AC, Flamm DL (1978) J Appl Phys 49:3796
58. Donnelly VM, Flamm DL, Dautremont-Smith WC, Werder DJ (1984) J Appl Phys 55:242
59. Egitto FD, Matienzo LJ, Schreyer HB (1992) J Vac Sci Technol A 10:3060
60. Legtenberg R, Jansen H, de Boer M, Elwenspoek M (1995) J Electrochem Soc 142:2020
61. Xia YN, Whitesides GM (1998) Angew Chem Int Ed 37:551
62. Li HW, Huck WTS (2002) Curr Opin Solid State Mat Sci 6:3
63. Granlund T, Nyberg T, Roman LS, Svensson M, Inganas O (2000) Adv Mater 12:269
64. Clarson SJ, Semlyen JA (1993) Siloxane polymers. Prentice-Hall, New York
65. Delamarche E, Geissler M, Bernard A, Wolf H, Michel B, Hilborn J, Donzel C (2001) Adv Mater 13:1164
66. Hillborg H, Gedde UW (1998) Polymer 39:1991
67. Chua DBH, Ng HT, Li SFY (2000) Appl Phys Lett 76:721
68. Bowden N, Brittain S, Evans AG, Hutchinson JW, Whitesides GM (1998) Nature 393:146
69. Lammertink RGH, Korczagin I, Hempenius MA, Vancso GJ (2004) Metal-containing polymers for high-performance resist applications. In: Abd-El-Aziz AS, Carraher CE, Pittman CU, Sheats JE, Zeldin M (eds) Macromolecules containing metal and metal-like elements, vol 2. Wiley, New York, p 115–133
70. Efimenko K, Wallace WE, Genzer JJ (2002) J Colloid Interface Sci 254:306
71. Wang MT, Braun HG, Kratzmuller T, Meyer E (2001) Adv Mater 13:1312
72. Suh KY, Kim YS, Lee HH (2001) Adv Mater 13:1386
73. Suh KY, Lee HH (2002) Adv Funct Mater 12:405
74. Bates FS, Rosedale JH, Fredrickson GH (1990) J Chem Phys 92:6255
75. Hamley IW Nanotechnology 14:R39
76. Park C, Yoon J, Thomas EL (2003) Polymer 44:6725
77. Eitouni HB, Balsara NP, Hahn H, Pople JA, Hempenius MA (2002) Macromolecules 35:7765
78. Coulon G, Russell TP, Deline VR, Green PF (1989) Macromolecules 22:2581
79. Coulon G, Ausserre D, Russell TP (1990) Journal de Physique 51:777
80. Lammertink RGH, Hempenius MA, Vancso GJ, Shin K, Rafailovich MH, Sokolov J (2001) Macromolecules 34:942
81. Lammertink RGH, Hempenius MA, Vancso GJ (2000) Langmuir 16:6245
82. Park M, Harrison C, Chaikin PM, Register RA, Adamson DH (1997) Science 276:1401
83. Spatz JP, Herzog T, Mößmer S, Ziemann P, Möller M (1999) Adv Mater 11:149
84. Spatz JP, Eibeck P, Mößmer S, Möller M, Herzog T, Ziemann P (1998) Adv Mater 10:849
85. Segalman RA, Yokoyama H, Kramer EJ (2001) Adv Mater 13:1152
86. Cheng JY, Ross CA, Thomas EL, Smith HI, Vancso GJ (2002) Appl Phys Lett 81:3657
87. Neuse EW, Khan FBD (1986) Macromolecules 19:269
88. Kelch S, Rehahn M (1999) Macromolecules 32:5818

89. Decher G (1997) Science 277:1232
90. Bertrand P, Jonas A, Laschewsky A, Legras R (2000) Macromol Rapid Commun 21:319
91. Wu A, Yoo D, Lee JK, Rubner MF (1999) J Am Chem Soc 121:4883
92. Hodak J, Etchenique R, Calvo EJ, Singhal K, Bartlett PN (1997) Langmuir 13:2708
93. Sun J, Sun Y, Zou S, Zhang X, Sun C, Wang Y, Shen J (1999) Macromol Chem Phys 200:840
94. Hempenius MA, Robins NS, Péter M, Kooij ES, Vancso GJ (2002) Langmuir 18:7629
95. Halfyard J, Galloro J, Ginzburg M, Wang Z, Coombs N, Manners I, Ozin GA (2002) Chem Commun 1746
96. Beh WS, Kim IT, Qin D, Xia YN, Whitesides GM (1999) Adv Mater 11:1038
97. Clark SL, Handy ES, Rubner MF, Hammond PT (1999) Adv Mater 11:1031
98. Schanze KS, Bergstedt TS, Hauser BT, Cavalaheiro CSP (2000) Langmuir 16:795
99. Rulkens R, Lough AJ, Manners I, Lovelace SR, Grant C, Geiger WE (1996) J Am Chem Soc 118:12683
100. Foucher D, Ziembinski R, Petersen R, Pudelski J, Edwards M, Ni YZ, Massey J, Jaeger CR, Vancso GJ, Manners I (1994) Macromolecules 27:3992
101. Foucher DA, Honeyman CH, Nelson JM, Tang BZ, Manners I (1993) Angew Chem Int Ed 32:1709
102. Finklea HO (1996) Electrochemistry of organized monolayers of thiols and related molecules on electrodes. In: Bard AJ, Rubinstein I (eds) Electroanalytical chemistry, vol 19. Dekker, New York, p 109
103. Murray RW (1984) Chemically modified electrodes. In: Bard AJ (ed) Electroanalytical chemistry, vol 13. Dekker, New York, p 191
104. Decher G, Lehr B, Lowack K, Lvov Y, Schmitt J (1994) Biosens Bioelectron 9:677
105. Hammond PT, Whitesides GM (1995) Macromolecules 28:7569
106. Clark SL, Hammond PT (1998) Adv Mater 10:1515
107. Clark SL, Hammond PT (2000) Langmuir 16:10206
108. Sprik M, Delamarche E, Michel B, Rothlisberger U, Klein ML, Wolf H, Ringsdorf H (1994) Langmuir 10:4116
109. Cheng JY, Mayes AM, Ross CA (2004) Nature Materials 3:823